TU Delft

Delft University of Technology

Magnetic Coupling Based Test Development for Contact and Interconnect Defects in STT-MRAMs

Yuan, S.; Zhang, Z.; Fieback, M.; Xun, H.; Marinissen, E. J.; Kar, G. S.; Rao, S.; Couet, S.; Taouil, M.; Hamdioui, S.

DOI
10.1109/ITC51656.2023.00040

Publication date
2023

Document Version
Final published version

Published in
Proceedings - 2023 IEEE International Test Conference, ITC 2023

Citation (APA)
Yuan, S., Zhang, Z., Fieback, M., Xun, H., Marinissen, E. J., Kar, G. S., Rao, S., Couet, S., Taouil, M., & Hamdioui, S. (2023). Magnetic Coupling Based Test Development for Contact and Interconnect Defects in STT-MRAMs. In *Proceedings - 2023 IEEE International Test Conference, ITC 2023* (pp. 236-245). (Proceedings - International Test Conference). IEEE. https://doi.org/10.1109/ITC51656.2023.00040

Important note
To cite this publication, please use the final published version (if applicable).
Please check the document version above.

Copyright
Other than for strictly personal use, it is not permitted to download, forward or distribute the text or part of it, without the consent of the author(s) and/or copyright holder(s), unless the work is under an open content license such as Creative Commons.

Takedown policy
Please contact us and provide details if you believe this document breaches copyrights.
We will remove access to the work immediately and investigate your claim.

This work is downloaded from Delft University of Technology.
For technical reasons the number of authors shown on this cover page is limited to a maximum of 10.

Green Open Access added to TU Delft Institutional Repository

'You share, we take care!' - Taverne project

https://www.openaccess.nl/en/you-share-we-take-care

Otherwise as indicated in the copyright section: the publisher
is the copyright holder of this work and the author uses the
Dutch legislation to make this work public.

Magnetic Coupling Based Test Development for Contact and Interconnect Defects in STT-MRAMs

S. Yuan*‡ Z. Zhang* M. Fieback* H. Xun* E. J. Marinissen‡ G. S. Kar‡
S. Rao‡ S. Couet‡ M. Taouil*† S. Hamdioui*†
*TU Delft, Delft, The Netherlands †CognitiveIC, Delft, The Netherlands ‡IMEC, Leuven, Belgium
{S.Yuan-4, M.C.R.Fieback, H.Xun, M.Taouil, S.Hamdioui}@tudelft.nl {ziweizhang0808}@gmail.com
{Erik.Jan.Marinissen, Gouri.Kar, Siddharth.Rao, Sebastien.Couet}@imec.be

***Abstract*—The development of Spin-Transfer Torque Magnetic RAMs (STT-MRAMs) mass production requires high-quality test solutions. Accurate and appropriate fault modeling is crucial for the realization of such solutions. This paper targets fault modeling and test generation for all interconnect and contact defects in STT-MRAMs and shows that using the defect injection and circuit simulation for fault modeling without incorporating the impact of magnetic coupling will result in an incomplete set of fault models; hence, not obtaining accurate fault models. Magnetic coupling introduced by the stray field is an inherent property of STT-MRAMs and may foster the occurrence of additional memory faults. Not considering the magnetic coupling clearly will give rise to test escapes. The paper introduces a compact model for STT–MRAM that incorporates the intra- and inter-cell stray field, uses this model to derive the full set of fault models for interconnect and contact defects, and finally proposes an efficient test solution.**

***Index Terms*—STT-MRAM, stray field, magnetic coupling, fault modeling, test development.**

I. Introduction

Spin-Transfer Torque Magnetic RAMs (STT-MRAMs) have emerged as a promising technology thanks to their competitive write performance, low power consumption, retention, and endurance [1]. Since its early commercialization in 2006, world-leading foundries and producers (such as TSMC, Samsung, Intel, and Everspin) have entered the MRAM market, leading to a substantial increase in single-chip storage capacity from 4 MB to 1 GB [1–5]. Testing of such chips is a must in order to guarantee the customer-required quality.

Prior works on fault modeling and testing for STT-MRAMs can be classified into two types: testing of *conventional* defects and testing of *unique* defects in Magnetic Tunneling Junctions (MTJs). Testing of conventional defects, like interconnect and contact defects [6–11], assume that such defects can be modeled as *linear resistance*, similar to what has been used for defects in DRAMs and SRAMs [12,13]. However, testing of unique defects in the MTJ such as the pinhole [14–16] used device-aware testing (DAT) [15,16]; DAT incorporates the impact of physical defects into the technology parameters of the device and thereafter in the electrical parameters in order to develop a compact model of a defective MTJ device. The model is subsequently used for fault analysis to derive appropriate fault models and thereafter test solutions. DAT considers the impact of *magnetic coupling* due to the stray field [15] inherently introduced by MTJ ferromagnetic layers [17]. However, this is not completely the case for the work reported on testing conventional defects [7–9]. For instance, in such work memory *coupling faults* are derived by simulating Bridges [12] between adjacent memory cells; such defects cause the *electrical effect* through unwanted current paths. Yet the magnetic coupling could also play a role and foster the occurrence of such coupling faults for STT-MRAMs. Previous works on conventional defects have either included only the electrical effect due to defects [6,7], or included only magnetic coupling while ignoring the electrical effect [8–10], making the analysis not complete. Therefore, incorporating the impact of stray field/coupling in the presence of interconnect and contact defects within a single cell or between cells is essential for accurate fault modeling and appropriate test development.

This paper advances the state-of the art by proposing a systematic approach to analyze all possible interconnect and contact defects in STT-MRAMs while appropriately incorporating the *impact of stray field/magnetic coupling* of such devices. The results show, for example, that the magnetic coupling causes additional coupling faults in the presence of defects; these are not sensitized when considering only the electrical effect of defects. Hence, involving magnetic coupling for fault modeling and test development reduces the number of escapes and improves the outgoing product quality. In brief, the contributions of the paper are as follows:

- Discussion of the electrical effect of defects versus stray field/coupling in STT-MRAMs.
- Model for the intra- and inter-cell magnetic stray field in STT-MRAMs that will be used for defect injection and circuit simulation.
- Systematic derivation of fault models for all interconnect and contact defects in STT-MRAMs (modeled as resistors) while considering both their electrical effect as well as the presence of magnetic coupling.
- Test solutions for all derived fault models.

The rest of this paper is organized as follows. Section II introduces the STT-MRAM basics. Section III discusses both the electrical effect of defects and the magnetic coupling in STT-MRAMs. Section IV derives a model for the magnetic coupling in defect-free STT-MRAMs. Section V establishes the defect space. Section VI describes the fault modeling methodology. Section VII derives the fault models for all contact and interconnect defects in STT-MRAMs. Section VIII proposes a method for test development and uses it to obtain an optimal test solution for all derived faults. Section IX concludes this paper.

2023 IEEE International Test Conference (ITC) | 979-8-3503-4325-0/23/$31.00 ©2023 IEEE | DOI: 10.1109/ITC51656.2023.00040

2378-2250/23/$31.00 ©2023 IEEE
DOI 10.1109/ITC51656.2023.00040

Authorized licensed use limited to: TU Delft Library. Downloaded on January 30,2024 at 07:06:06 UTC from IEEE Xplore. Restrictions apply.

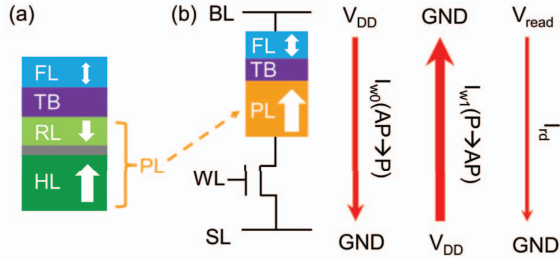

Fig. 1. (a) Simplified MTJ stack, (b) 1T-1M cell.

II. Background

In this section, we introduce the basics of the MTJ device, the STT-MRAM cell, and the framework of test development.

A. MTJ device

The fundamental data-recording element in STT-MRAMs is the MTJ; it demonstrates the one-bit data storage by encoding two bi-stable resistance states.

Fig. 1(a) presents a simplified schematic of an MTJ [15]. Typically, the MTJ consists of an ultra-thin dielectric Tunnel Barrier (TB) sandwiched between the Free Layer (FL) and the Pinned Layer (PL). The FL is a thin ferromagnetic layer (e.g. $1\,\mathrm{nm}$), whose magnetization can be switched through write operations. The TB is a thin insulator made of MgO, the thickness of which is around $1\,\mathrm{nm}$. The PL is a multiple-layer stack composed of a thin Reference Layer (RL), a thin metal spacer, and a thick Hard Layer (HL). The RL is a ferromagnetic layer that is anti-ferromagnetically coupled to the HL through the spacer, resulting in opposite magnetization directions between the two layers. The HL is thick and stable, which ensures the stability of the RL. For defect-free devices, the whole PL is stable and never switches.

When a current flows through the device, it offers STT to the FL, which may switch the FL magnetization to be either parallel or anti-parallel to that of the RL. The MTJ resistance is determined by the FL magnetization direction: when the FL and the RL magnetization are in parallel, the MTJ presents low resistance (R_P), described as P state or '0' state; otherwise, when the magnetization of the FL and the RL are anti-parallel, the MTJ is in high resistance, described as AP state or '1' state. The Tunneling Magneto-Resistance, presented as $TMR = (R_{AP} - R_P)/R_P$, is applied to present the ratio between R_P and R_{AP} [18]. A high-performance MTJ requires a high TMR (usually larger than 2 [18]).

B. 1T-1M STT-MRAM cell

Fig. 1 (b) illustrates the structure and write/read operations of a bottom-pinned 1 Transistor - 1 Magnetic Tunnel Junction (1T-1M) bit cell The cell comprises an N-type Metal-Oxide-Semiconductor Field-Effect Transistor (MOSFET) selector and an MTJ, with three terminals connecting to the Bit Line (BL), Source Line (SL), and Word Line (WL), respectively. During write operations, the voltage of WL selects the cell and the voltage between BL and SL controls the operation type. For instance, the $1w0$ operation refers to connecting BL to V_{DD}, and SL to ground, generating a writing current I_{w0} flowing through the MTJ device from the FL to the PL, and switching the MTJ state from AP to P. The tunneling electrons provide STT that switches the FL magnetization from parallel to anti-parallel to that of the RL. On the contrary, a $0w1$ operation refers to offering an opposite current I_{w1} by connecting BL to ground and SL to V_{DD}. The MTJ state is switched from P→AP by the reversed Spin Transfer Torque (STT). Notice that we use the same V_{DD} for both write operations, yet R_P is smaller than R_{AP}. Hence, $I_{\mathrm{w1}}(P \rightarrow AP)$ is usually larger than $I_{\mathrm{w0}}(AP \rightarrow P)$. For write operations, a writing current I_{w} larger than the critical current I_{c} is necessary to achieve a high write success rate, and the switching time t_{w} is inversely proportional to $I_{\mathrm{w}} - I_{\mathrm{c}}$ [18]. In read operations, a read current I_{rd} being much smaller than I_{c} is offered to detect the MTJ resistance while avoiding unwanted state switches. The sense amplifier is employed to detect the device state, leading to a short read time t_{rd} (e.g. $5\,\mathrm{ns}$) [19].

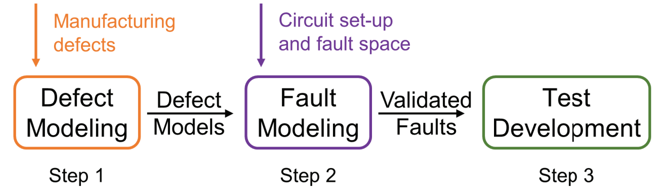

Fig. 2. Framework of STT-MRAM test development

C. Framework of the STT-MRAM test design

Fig. 2 illustrates the three-step framework for the STT-MRAM test development, which provides a systematic method to design a manufacturing test to detect defects [20]. Step 1 'defect modeling', refers to modeling manufacturing defects. Conventional defects like contact and interconnect defects can be modeled as resistors. For example, an unexpected superfluous piece of metal connecting two nodes can be modeled as an additional resistive path between these two nodes. Besides, Wu *et al.* identified unique defects in the MTJ, which can be modeled only by the DAT method, such as done for the pinhole [16]. Step 2 'fault modeling', defines the fault space and validates it through defect injection and circuit simulation. Step 3 'test development', generates test solutions to detect the validated faults.

In this paper, we will use this three-step approach to develop test solutions for interconnect and contact defects, which may cause unwanted current paths and thus result in coupling faults in STT-MRAMs, but then by considering the impact of magnetic coupling as well. Note that the magnetic coupling is generated by the nature of the MTJ; hence, it cannot be ignored. We use regular resistors to model interconnect and contact defects [12].

III. Importance of Considering Magnetic Coupling for Fault Modeling

Next, we briefly discuss the magnetic coupling and how it can foster or impede the occurrence of faults in the presence of defects such as Bridges between two cells.

Authorized licensed use limited to: TU Delft Library. Downloaded on January 30,2024 at 07:06:06 UTC from IEEE Xplore. Restrictions apply.

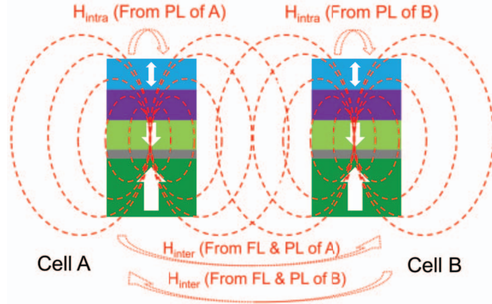

Fig. 3. Stray field of TMJ

A. STT-MRAM stray field and magnetic coupling

Even when the STT-MRAM works in an ideal environment without any external magnetic field, extra magnetic field introduced by the MTJ ferromagnetic layers, named the 'stray field', still exists [6]. As shown in Fig. 3, the stray field consists of the *intra-cell* stray field originating from the PL of the cell itself, and the *inter-cell* stray field generated by the FL and the PL of neighboring cells [15]. Note that *magnetic coupling* between cells is attributed to the inter-cell stray field [6,15]. Since PL is stable and never switches, the PL-introduced stray field never changes, thus its contribution to the magnetic coupling is constant. However, the FL-introduced inter-cell stray field is cell-state dependent; it will be oriented to be reversed with the MTJ state switching.

B. Electrical effect due to the presence of defects

In the presence of a defect in an STT-MRAM, an unwanted electrical effect may take place. As an example, Fig. 4 shows a Bridge defect (modeled as a resistor) between two adjacent cells in the same row. Due to the defect, an unwanted current path can take place, resulting in memory *coupling faults*. Coupling faults are defined as faults involving two cells, say the *aggressor* cell and the *victim* cell where the fault shows up. To sensitize coupling faults, specific Data-Background (DB) may be needed; DB is the patterns of ones and zeros as seen in the memory array [20].

C. Electrical effect in the presence of magnetic coupling

As already mentioned, a defect in a memory cell or between adjacent memory cells can cause faults. For conventional memory types, such as DRAMs and RRAMs, the fault modeling only needs to include the electrical effect of the defect on the behavior of the memory. However, this is not enough when considering fault modeling for STT-MRAMs. Due to the nature of such technology, it gives rise to both the intra- and inter-cell stray field, which may foster the sensitization of faults in the presence of even *weak defects*. Here, weak defects are defined as defects that are not strong enough to sensitize faults when considering only their electrical impact. Hence, not considering the impact of magnetic coupling for fault modeling may lead to escapes. The impact of the stray field must be considered for accurate and appropriate STT-MRAM fault modeling to generate high-quality test solutions.

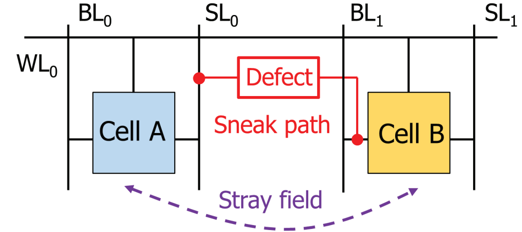

Fig. 4. Magnetic coupling in the presence of a Bridge defect

Fig. 4 shows also that in addition to the unwanted current path created by the Bridge defect, the inter-cell stray field may contribute with additional current resulting in e.g., a coupling fault. The table below shows the contributors to the sensitization of faults in STT-MRAMs (electrical effect versus stray field) and how they differ from each other.

Source type	Existence	Magnitude	Affect which behavior?
Electrical effect	Only in presence of a defect	Depends on defect strength	Read and write
Stray field	Always exists	Depends on cell state	Only write

The electrical effect may exist only when there is a defect; such a defect may or may not cause a fault depending on its strength. Besides, the electrical effect may cause faulty writes and/or reads as it affects the circuit current flow through the MTJ. The stray field always exists regardless of defects since the stray field is inherent to the MTJ ferromagnetic layers. Such a field may impact only write operations yet never impact read operations as will be shown in the next section. Note that the electrical effect and the magnetic coupling impact never affect each other, since they have independent origins and working mechanisms, yet they may work together contributing to the sensitization of a fault in STT-MRAM during write operations.

IV. Set-up of Magnetic Coupling

To study the magnetic coupling effect on the STT-MRAM test, it is necessary to model and incorporate it in a defect-free STT-MRAM array. In this section, we first introduce the MTJ model involving the stray field [15]. As this model cannot be directly applied to flexibly present the magnetic coupling effect in circuit-level simulations due to its low compatibility, we propose a new approach to directly implant the magnetic coupling into the STT-MRAM array, by converting it to the 'equivalent current source'. Finally, we present some simulation results of the model.

A. Stray field implantation in the MTJ model

In 2020, Wu *et al.* proposed the MTJ compact model considering the stray field effect; he adjusted the calculation of key electrical parameters, being the critical current (I_c) and average switching time (t_w), by incorporating the impact of the stray field (H_s) [15]. H_s exercised on a cell in the STT-MRAM array can be calculated by simply adding up the intra-cell stray

Authorized licensed use limited to: TU Delft Library. Downloaded on January 30,2024 at 07:06:06 UTC from IEEE Xplore. Restrictions apply.

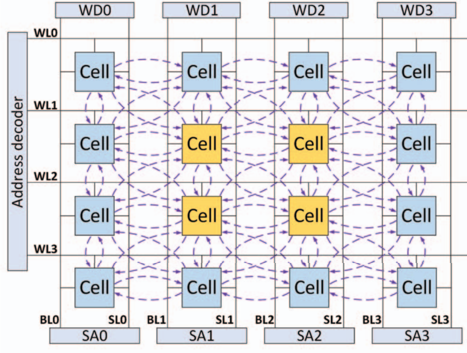

Fig. 5. Illustration of of magnetic coupling in 4x4 STT-MRAM array

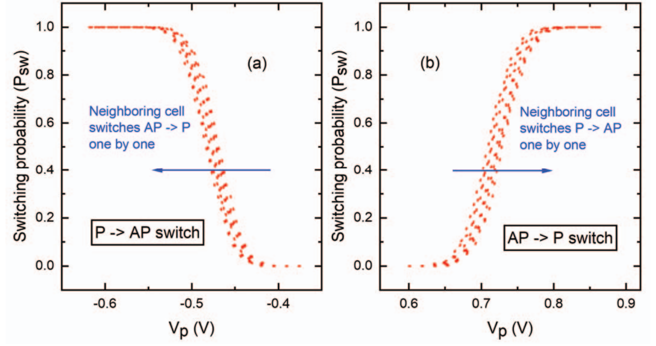

Fig. 6. MTJ behavior dependency on magnetic coupling effects

field ($H_{s-intra}$) and the sum of all of the PL-/FL-introduced inter-cell stray field ($H_{s-inter-PL}$, $H_{s-inter-FL}$):

$$H_s = H_{s-intra} + \sum(H_{s-inter-PL} + H_{s-inter-FL}) \quad (1)$$

Since the inter-cell stray field intensity is inversely proportional to the distance between devices, here we restrict ourselves only to the stray field generated by the eight physical neighboring devices (see also Fig. 5). The two key electrical parameters I_c and t_w can be then presented as [15]:

$$t_w = \frac{\left(C + \ln\left(\frac{\pi^2}{4}\Delta\right)\right) * e * m}{4 * \mu_B * \eta * (I_{MTJ} - I_c)}$$
$$I_c = \frac{1}{\eta} * \frac{\alpha e}{\hbar} * A * t_{FL} * M_s * (H_k + H_s) \quad (2)$$

where the symbols used in the equation are described in the table below.

C	Euler constant	Δ	Thermal stability
e	unit charge	m	FL magneton
μ_B	Bohr magneton	η	STT efficiency
I_{MTJ}	Current through the MTJ	α	Damping factor
$\hbar$	Reduced Planck constant	A	Cross-area
t_{FL}	Thickness of the FL	M_{s}	Saturation magnetization
H_{k}	Anisotropy magnetic field		

B. Magnetic coupling set-up in the STT-MRAM array

Although the MTJ compact model successfully incorporates the stray field effect, it cannot be directly applied to study the magnetic coupling effect on fault modeling. This model is based on the calculation of the magnetic field, which cannot be flexibly simulated by Spice. For example, when one MTJ state switches, the inter-cell stray field it offers to all of its neighboring cells is changed as well. However, this change cannot be directly reflected in the MTJ compact model; it may result in inaccurate simulation results. In order to accurately incorporate the magnetic coupling effect into the defective STT-MRAMs, we need to make the stray field calculation compatible with circuit-level simulations.

Next, we introduce a novel approach for modeling magnetic coupling effects by extracting the inter-cell stray field impact from the MTJ model and incorporating it into circuit-level simulations. We achieve this by transforming the stray field effect into an '*equivalent current source*'.

Conventionally, I_{MTJ} is converted to the 'equivalent magnetic field (H_{eq})' to design the MTJ compact model, presented as follows [21]:

$$H_{eq} = \frac{I_{MTJ} * \eta * \hbar}{2 * m * e * \alpha} \quad (3)$$

We use Eq. 3 to derive the current contribution due to the inter-cell stray field by transforming this field into 'MTJ-state-controlled equivalent current ($I_{s-inter}$)'. This can be carried out by replacing H_{eq} with $H_{s-inter}$, and reversing Eq. 3, presented as follows:

$$I_{s-inter} = \frac{2 * m * e * \alpha * H_{s-inter}}{\eta * \hbar}$$
$$H_{s-inter} = \begin{cases} H_{s-inter-PL} - H_{s-inter-FL} & \text{(P)} \\ H_{s-inter-PL} + H_{s-inter-FL} & \text{(AP)} \end{cases} \quad (4)$$

In this way, we extract the inter-cell stray field impact out of the MTJ model, and convert it to an equivalent (virtual) current source. The current source is realized by Verilog-A: the input is the state of one cell, and the output connects to the physical neighboring cell. By applying this virtual current source, the magnetic coupling is implanted into the STT-MRAM array. The key electrical parameters I_c and t_w of the MTJ model are adjusted to be:

$$t_w = \frac{\left(C + \ln\left(\frac{\pi^2}{4}\Delta\right)\right) * e * m}{4 * \mu_B * \eta * (\sum(I_{s-inter}) + I_{MTJ} - I_c)}$$
$$I_c = \frac{1}{\eta} * \frac{\alpha e}{\hbar} * A * t_{FL} * M_s * (H_k + H_{s-intra}) \quad (5)$$

Here, the $\sum(I_{s-inter})$ refers to the magnetic coupling effect introduced by the eight neighboring cells; its value is affected by the state of the neighboring cell, yet regardless of the defects. On the other hand, the I_{MTJ} may be affected by defects. In Eq. 5, we observe that $\sum(I_{s-inter})$ and I_{MTJ} never affects each other; the STT and the magnetic coupling are independent. Besides, their impact on the MTJ state switching can be evaluated by simply adding them up. Notice that we do not change the core method and math calculations in Eq. 2, yet make it possible to directly evaluate the magnetic coupling effect through circuit simulations.

Authorized licensed use limited to: TU Delft Library. Downloaded on January 30,2024 at 07:06:06 UTC from IEEE Xplore. Restrictions apply.

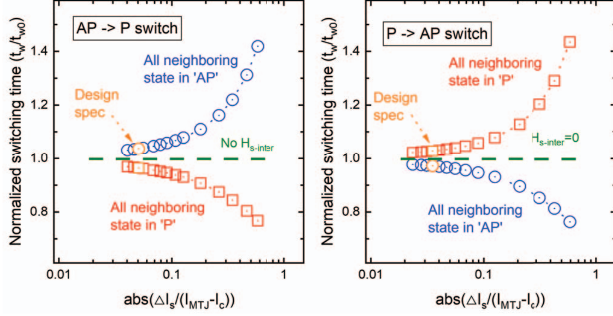

Fig. 7. Magnetic coupling effect with ΔI_{MTJ} becomes closer to I_c

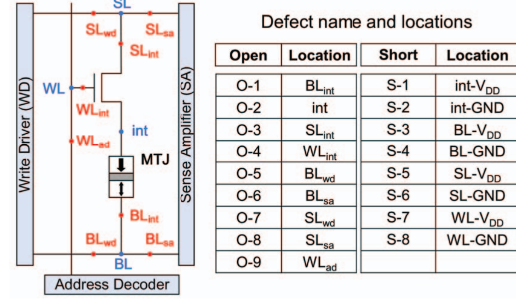

Open	Location	Short	Location
O-1	BL_{int}	S-1	int-V_{DD}
O-2	int	S-2	int-GND
O-3	SL_{int}	S-3	BL-V_{DD}
O-4	WL_{int}	S-4	BL-GND
O-5	BL_{wd}	S-5	SL-V_{DD}
O-6	BL_{sa}	S-6	SL-GND
O-7	SL_{wd}	S-7	WL-V_{DD}
O-8	SL_{sa}	S-8	WL-GND
O-9	WL_{ad}		

Fig. 8. Defect space of the Open and Short defects

In this section, we only talk about the MTJ switching model in the precessional regime, while ignoring the dynamic and thermal activation regime [22]. All read and write operations in this work only apply short pulses, hence the device works exclusively in the precessional regime [15,22]. A similar method may be applied in the dynamic and thermal activation regime by adding $I_{s-inter}$ into the calculation of t_w in these regimes, but it is beyond the scope of this work.

C. Defect-free STT-MRAM circuit set-up and simulation

In this study, we perform all the circuit-level simulations based on the 4×4 1T-1M STT-MRAM array, as presented in Fig. 5. In the array, cells in the same row share the same WL, and cells in the same column share the same BL and SL. The peripheral circuit consists of the write driver, address decoder, and sense amplifier. In addition to the regular circuit set-up, we implant the ‘equivalent current sources’ in this array. Here, the purple dashed lines are the ‘equivalent (virtual) current sources’, which are determined only by the state of the device, as given in Eq. 4), and modeled with Verilog-A. As a result, each MTJ controls eight current sources to all its neighboring cells to model the inter-cell stray field impact. The Cadence Spectre is adopted for circuit-level simulations. The Predictive Technology Model (PTM) 65-nm transistor library is applied in the simulation [23]. In this work, the Critical Diameter (CD) of the MTJ is $60\,\mathrm{nm}$, and the pitch (distance between neighboring cells in the same row or the same column) is $90\,\mathrm{nm}$. The MTJ model is calibrated with measurement data, and the circuit is verified to be fault-free with regular write/read operations [15].

Fig. 6 presents the magnetic coupling impact on the MTJ writing performance using the circuit set-up in Fig. 5. We extract the MTJ switching probability P_{sw} by varying the write pulse height V_p with constant pulse width. Fig. 6 (a) shows that when the eight neighboring cell states are switched from ‘1’ to ‘0’ one by one, the MTJ gradually requires a higher V_p for P→AP switching; when the neighboring cell states are in ‘0’, the $w0$ operation is favored. A complementary phenomenon for AP→P switching is shown in Fig. 6 (b).

The model design in this section enables us to qualitatively analyze the magnetic coupling effect on STT-MRAM write behaviors. Note that the magnetic coupling always plays a role in the MTJ switching performance regardless of the defects; it should have a negligible impact on the defect-free MTJ switching. For the reliable and robust STT-MRAM design, $\sum(I_{s-inter}) \ll (I_{MTJ}-I_c)$ [17]. However, in the presence of defects, I_c may become closer to I_{MTJ}, resulting in a stronger impact of $I_{s-inter}$ on t_w, as presented in Eq. 5. Here, we consider the two extreme situations: a) induced current when all the eight neighboring cells are in P state, b) induced current when all the eight neighboring cells are in AP state, and we define ΔI_s as the subtraction value of $\sum(I_{s-inter})$ in these two cases as:

$$\Delta I_s = \sum(2 * \frac{1}{\eta} * \frac{\alpha e}{\hbar} * A * t_{FL} * M_s * H_{s-inter-FL}) \quad (6)$$

Fig. 7 shows the dependency the magnetic coupling effect on $\Delta I_s/(I_{MTJ} - I_c)$. As $\Delta I_s/(I_{MTJ} - I_c)$ increases due to a defect, the normalized switching time (t_w/t_{w0}) gap between two extreme cases becomes larger, suggesting a defect may amplify the magnetic coupling effects on the STT-MRAM writing operation. It is worth noting that magnetic coupling has negligible impact on read operations; applying a small read voltage V_{rd} in the presence of the stray field will never cause the MTJ state to switch, as $(I_{MTJ} + I_{s-inter}) \ll I_c$.

V. Defect Space

In this section, the complete defect space of contact and interconnect defects is defined for STT-MRAMs. Here, the defect is modeled as resistors, which is commonly used [12]. Such defects can be classified as: 1) Open, an extra resistance within the connection; 2) Short, an undesired resistive path between the node and power supply; and 3) Bridge, an extra parallel resistance between two disconnected nodes. The defect strength is described by the resistance value ranging from $1\,\Omega$ to $10\,\mathrm{M}\Omega$. Note that whether all defined defects are realistic or not is strongly chip layout dependent [7]. Such information is barely published, and therefore in our analysis, we will cover the whole space.

A. Defect space of Open and Short defects

Although the 4×4 STT-MRAM array in Fig. 5 is applied for circuit simulations, we only inject the Short and Open defects in one cell for simplification, as presented in Fig. 8. Due to the symmetry, defects in different cells cause similar faults. For instance, the Open defects in different cells will cause these cells to fail in the same way.

Fig. 8 demonstrates the complete space of the Open and Short defects. The method of injecting the defect is as follows.

Authorized licensed use limited to: TU Delft Library. Downloaded on January 30,2024 at 07:06:06 UTC from IEEE Xplore. Restrictions apply.

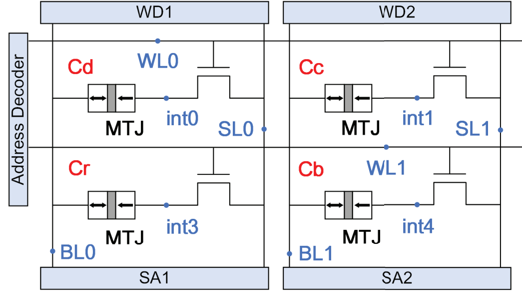

Defect name and locations

Bridge	Location	Bridge	Location	Bridge	Location
B-1	BL1-SL1	B-9	BL0-int4	B-17	int0-WL1
B-2	BL1-WL1	B-10	SL0-BL1	B-18	int0-int4
B-3	BL1-int4	B-11	SL0-SL1	B-19	WL1-int1
B-4	SL1-WL1	B-12	SL0-int4	B-20	int4-int1
B-5	SL1-int4	B-13	WL0-WL1	B-21	BL1-int3
B-6	WL1-int4	B-14	WL0-int4	B-22	SL1-int3
B-7	BL0-BL1	B-15	int0-BL1	B-23	int1-int3
B-8	BL0-BL1	B-16	int0-SL1		

Fig. 9. Defect space of the Bridge defects

Firstly, we present all four 'nodes' in the netlist of the 1T-1M cell: SL, WL, BL, int (the blue words in Fig. 8). The Open defect is presented as an extra resistance between the connected node and device, or between the connected node and peripheral circuit. For example, the defect O-8 is modeled as an extra resistance between the node SL and peripheral circuit SA. There are nine Open defects in total. The Short defect refers to the unexpected resistive path between the node and Power/GND, such as the S-2 (int-GND). With four nodes, there are a total of eight Short defects.

B. Defect space of Bridge defects

To simplify the simulation process, the Bridge defects are only injected in the 2×2 array, which is indicated by the yellow cells in Fig. 5. Due to the symmetry, faults sensitized by the Bridge defects in the 2×2 array actually can represent the faults sensitized by all the possible Bridge defects in the large-scale array [24]. The 2×2 array includes all three possible locations of adjacent cells: cells in the same row, cells in the same column, and cells in the same diagonal. Because the large scale m×n array can be treated as the repetition of 2×2 arrays, the same defect in different 2×2 arrays actually results in the same types of faults.

Fig. 9 demonstrates the complete defect space of the Bridge defects. The method of injecting the Bridge defect is as follows. We present all ten nodes in the 2×2 array (the blue words in Fig. 9). Since the Bridge indicates an extra parallel resistance between disconnected two nodes, we first injected all the possible defects between every two of the ten nodes. However, not all defects between the ten nodes need to be considered due to symmetry. For instance, with the existence of defect B-3 (BL1-int4), the Bridge defect between BL0-int0 is unnecessary to be considered. Therefore, we delete the repeating ones, and eventually get a total of 23 Bridge defects as shown in Fig. 9.

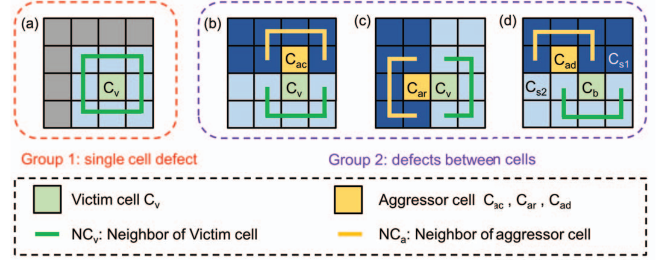

Fig. 10. Illustration of the DBs for the fault modeling methodology for (a) single cell defects and defects between adjacent cells.

VI. Fault Modeling Methodology

Next, we will describe the fault modeling methodology based on defect injection and circuit simulation. Note that all the defects are modeled as resistors; changing the strength of defects is done through changing the value of the resistance. The fault modeling is performed for two cases: for all defects in single cell, and for all defects between two adjacent cells. In addition, we investigated two scenarios for each case: with and without involvement of inter-cell stray field; this is in order to be able to investigate the impact of magnetic coupling in the presence of defects.

A. Methodology for single-cell defects

The simulation platform used is similar to that shown in Fig. 5. As two scenarios are considered, two versions of simulation platforms were generated: one using an MTJ model that incorporates only the intra-cell stray field (hence no inter-cell stray field), and one using an MTJ model that incorporates both intra- and inter-cell stray field. For each simulation platform, defects are injected, sensitizing operation sequences are applied to the defective cell (called victim-cell C_v), and the behavior of the C_v is observed. The performed sensitizing operations consist of '0' (state 0), '1', '$0w0$ (write 0 operation to C_v being initialized to 0)', '$0w1$', '$1w0$', '$1w1$', '$0r0$' (read 0 operation to a cell containing 0), '$1r1$'. When investigating the impact of defects in the absence of inter-cell stray field, the DB of the eight neighboring cells of C_v (the green line in Fig. 10 (a)) is irrelevant. However, this is relevant when considering the impact of magnetic coupling. For simplicity, while covering all possible impacts, we consider only two extreme cases for the DBs: all the eight neighboring cells are set to 0 or to 1; meaning using *solid* DB patterns [20].

B. Methodology for defects between cells

Similar to the last subsection, we apply two versions of simulation platforms: one including only the intra-cell stray field, and including both the intra- and inter-cell stray field. For each simulation platform, defects are injected between adjacent cells. We vary the defect strength and apply operations on the victim-cell C_v. Here, the other cell connected with C_v by the defect is called the aggressor-cell C_a, $a \in \{ac, ar, ad\}$; the state of C_a may affect the fault modeling. Depending on the defect location, Fig. 10 (b)-(d) present three types of C_a: 1) C_{ac}, the same column of C_v, 2)

Authorized licensed use limited to: TU Delft Library. Downloaded on January 30,2024 at 07:06:06 UTC from IEEE Xplore. Restrictions apply.

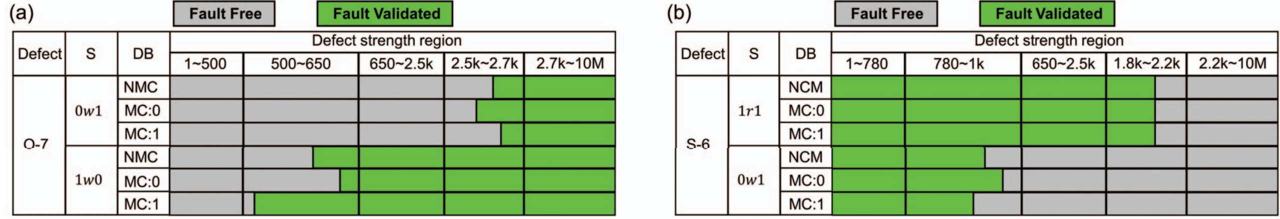

Fig. 11. Fault map of (a) the O-7 defect and (b) the S-6 defect

C_{ar}, the same row of C_v, 3) C_{ad}, the same diagonal of C_v. The behaviors of both C_v and C_a are observed while applying the operations on C_v, to perform the fault modeling.

When studying the impact of defects in the absence of magnetic coupling, we only need to include the electrical effect by setting the state C_a to be either '0' or '1'. For the platform including the magnetic coupling, we need to consider both the electrical effect and the magnetic coupling impact. Due to the independent origin of the electrical effect and the magnetic coupling impact, we can incoporate them one by one. Firstly, we set C_a state to include the electrical effect, then we consider the magnetic coupling. Because both C_v and C_a may be involved in coupling faults, we need to set their neighboring cells separately to fully include the magnetic coupling, as NC_v and NC_a presented in Fig. 10. For simplicity, we consider two extreme situations of NC_v and NC_a separately, with a total of four cases: (NC_v, NC_a) = (0, 0), (0, 1), (1, 0), (1, 1),.

Next, We combine our methodology with certain DB patterns which are applied in the industry test design [20]. Since the regular 'Row Stripe' and 'Column Stripe' patterns in [20] do not directly match our methodology, we use the 'Double-Row Stripe' and 'Double-column Stripe' patterns, as presented in Fig. 10. The 'Double-Row Stripe' pattern is applied for defects between C_v and C_{ac}, and the 'Double-Column Stripe' pattern is applied for defects between C_v and C_{ar} (Fig. 10 (b) - (c)). For cells that are neighboring both C_v and C_a, how to set them depends on the actual situation. For instance, in Fig. 10 (b), the cell on the diagonal of C_v and the same row of C_{ac} is treated as the NC_a, since the stray field from this cell has a stronger impact on C_{ac} than C_v. However, it is difficult to combine the DB pattern with cases when defects are between C_v and C_{ad}, since no proper DB pattern can properly distinguish the NC_v and NC_a cells. For example, Fig. 10 (d) presents the application of the 'Double-Row Stripe' pattern in this case, there are two specific cells C_{s1} and C_{s2} that cannot be grouped well: C_{s1} should belong to NC_v, yet in this pattern, it is the same state of to NC_a, the similar case occurs for C_{s2}. In this work, we temporarily ignore the two cells, and just simply apply the 'Double-Row Stripe' in Fig. 10 (d). Next section, we will apply the operations on C_v for all three cases for fault modeling first, then analyze the impact of the two cells, and show that it can be ignored.

VII. Fault modeling

In this section, we report on fault models obtained based on the methodology described in Section VI. We analyze and compare the impact of the electrical effect (due to defects) on the fault behavior of STT-MRAM both in the absence as well as in the presence of the magnetic coupling impact.

A. Validated faults for single cell defects

Fig. 11 (a) and (b) show two examples of fault maps summarizing the results of the fault analysis performed for the defects O-7, respectively, S-6 (see the table of Fig. 8). The fault map consists of (from left to right) the simulated defect, applied sensitizing operations S, DB (Data-background) used for the eight physical neighbor cells, and whether the faults are sensitized depends on the defect strength range. Here, NMC for DB indicates No Magnetic Coupling considered (i.e., $I_{s-inter}$ is not incorporated during the simulation), while MC:1 (MC:0) indicates that magnetic coupling is incorporated with all the neighboring cells of the C_v are set to 1 or 0. The 'green' boxes indicate ranges where faults are sensitized and the 'grey' ones indicate no faults sensitized. To clearly demonstrate the magnetic coupling impact and electrical effect, we make additional simulations to zoom in on the range around the border of green and grey boxes. Sequences not sensitizing any fault are not included here.

To maximize the test coverage, we need to consider the DB pattern and associated operations that can sensitize faults for the longest defect strength range; this has to be done for each defect. For example, Fig. 11 (a) reveals that the operation $1w0$ sensitizes the longest defect strength range of O-7 for MC:0, which is attributed to the magnetic coupling. When the neighboring cells are in state '1', the $0w1$ operation is favored since the magnetic coupling contributes to the switching process; it is modeled as the magnetic coupling contributes with a current $I_{s-inter}$ going in the same direction as that of I_{MTJ}. On the other hand, when the neighboring cells are in state '0', the $0w1$ operation is disfavored since I_{MTJ} and $I_{s-inter}$ are in opposite directions; hence, MC:1 enables more $1w0$ operations to fail for smaller defect sizes. The defect coverage for NMC case is always between that of the two extreme cases of MC:0 and MC:1. Hence, not considering the magnetic coupling will never provide maximal test coverage.

Fig. 11 (b) shows the magnetic coupling effect for S-6. For the $0w1$ operation, the longer defect strength range is sensitized for MC: 1. However, overall the longest defect strength range is sensitized by the $1r1$ operation, and it is the same for all the cases NMC, MC:1, and MC:0; this indicates that read operation is not affected by magnetic coupling, which is consistent with our analysis in Section III. Clearly that to maximize the defect coverage for S-6, the $1r1$ operation has to be used regardless of the DB pattern.

Authorized licensed use limited to: TU Delft Library. Downloaded on January 30,2024 at 07:06:06 UTC from IEEE Xplore. Restrictions apply.

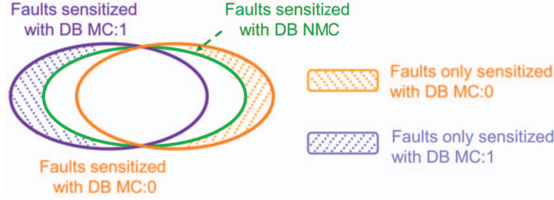

Fig. 12. Faults Venn diagram for all analyzed singe-cell defect

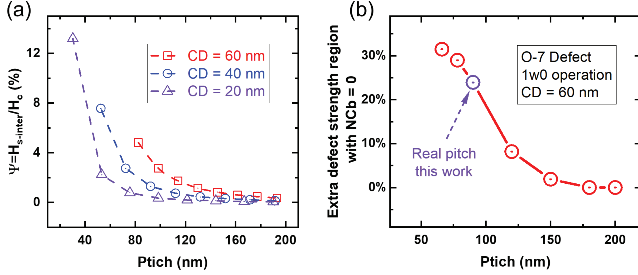

Fig. 13. Device size and pitch effect on magnetic coupling and fault modeling

Fig. 12 give the Venn diagram that summarized the results found when analyzing all single-cell defect for the three cases (NMC, MC:1 and MC:0). As it is shown in the figure, performing fault modeling without incorporating magnetic coupling will results in reduced validated fault space. Building test solutions based on this will obviously not lead to high-quality test solutions. Including the impact of magnetic coupling in the fault analysis fosters the sensitization of additional faults; some of these are DB dependent. As the figure shows, there are some faults that take place only at DB=0, and others only at DB=1. Hence, to obtain accurate fault models, it is crucial to incorporate magnetic coupling. Note that the results for NMC case can be seen as a 'middle state' between two extreme cases involving magnetic coupling.

We further investigate the dependency of the magnetic coupling effect on different device sizes and pitches. Fig. 13 (a) presents the pitch impact on Ψ (defined as the ratio of $H_{s-inter}$ on H_c (FL coercivity)) for different device sizes. Smaller devices or devices with smaller pitches suffer more from the impact of the inter-cell stray field, hence the magnetic coupling. For example, Fig. 13 (b) shows $1w0$ will fail for additional defect strength of O-7 in case the pitch is made smaller for MC:0 case (i.e., see also Fig. 11). This implies that with the device dimension scaling down, incorporating magnetic coupling for fault modeling and test development will become even more important. Note that the actual stray field intensity also depends on the device material, peripheral circuit design, and other factors.

B. Validated faults for defects between cells

Fig. 14 shows a fault map example for defects involving two cells; it reports the results of the defect B-19 which is a Bridge between the victim cell C_v and C_{ac} being the aggressor cell in the same column (see also the table of Fig. 8). The same notation is used as for Fig. 11; the added column 'Sate C_{ac}' provides the state of the $aggressor cell$. Note that the DB column now consists of five cases per state of C_{ac}: NMC,

Fault Free | Fault Validated

Defect	S	C_{ac} State	DB	Defect strength region: 1~6k	6-8k	650~2.5k	8~200k	200k~10M
B-19	0w1	0	NMC					
			MC:(0,0)					
			MC:(0,1)					
			MC:(1,0)					
			MC:(1,1)					
		1	NMC					
			MC:(0,0)					
			MC:(0,1)					
			MC:(1,0)					
			MC:(1,1)					
	1r1	0	MC:(-,-)					
		1	MC:(-,-)					

Fig. 14. Fault map of defect B-19

and four extreme cases providing MC the DB patterns for both NC_v (5 neighbor cells of the victim cell) and NC_a (5 neighbor cells of the aggressor cell); see Fig. 10. The '-' indicates that the fault model is DB-independent.

As presented in Fig. 14, the longest defect strength range is sensitized only by the $1r1$ operation with the C_{ac} state in '1'; the electrical effect (unexpected current path) plays a role in this case. Besides, this fault is independent of the DB pattern, as the magnetic coupling never affects the read operation. On the other hand, while the faults with the '0w1' operation definitely relate to the magnetic coupling, it is uncertain if the unexpected current path is also involved unless we make additional efforts to analyze the detailed circuit (it is involved in this case). Note that to detect this defect, only the $1r1$ operation is required irrespective of the DB pattern. Hence, the magnetic coupling is not involved in detecting B-19.

Additionally, we present how to deal with cells C_{s1} and C_{s2} in Fig. 10 (d). If read operations sensitize a much longer defect strength range than write operations, we ignore the impact of the two cells. Otherwise, extra simulations are carried out by switching the state of C_{s1} and C_{s2}. In this work, the impact of these two cells is disregarded.

By the analysis in this section, we show that the electrical effect and magnetic coupling impact on STT-MRAM faulty behaviors can be either independent or combined. As shown in Fig. 11 and Fig.14, detecting the defect O-7 requires only considering the magnetic coupling; detecting the defect B-19 requires only considering the electrical effect; and both effects are not considered in detecting the defect S-6. Therefore, to obtain a high-quality STT-MRAM test to detect all validated faults, both of the electrical effect and the magnetic coupling impact need to be carefully included during the test design.

VIII. Test Solution

A high-quality march test solution requires sensitizing all validated faults with the lowest cost. To achieve this, we need to select the proper sequence and DB while considering both the electrical effect and magnetic coupling impact. In this section, we firstly introduce the 'DB-Based Integer Linear Programming (DB-ILP)', as a mathematical method improved from the primary ILP with the incorporation of DB patterns [24]. Then, We apply this method to our fault models, generate an ideal march test algorithm, and verify its effectiveness.

Authorized licensed use limited to: TU Delft Library. Downloaded on January 30,2024 at 07:06:06 UTC from IEEE Xplore. Restrictions apply.

TABLE I. EXAMPLE TO DB-ILP TABLE

			DB pattern, $\mathrm{DB}_{\mathrm{m,\ for\ m:1\to M}}$													$\sum_{m=1}^{M}\sum_{n=1}^{N} a_{k,l,m,n}$
			DB_1				DB_2				...	DB_M				
			$\mathrm{S}_{\mathrm{1,n,\ for\ n:1\to N}}$				$\mathrm{S}_{\mathrm{2,n,\ for\ n:1\to N}}$				...	$\mathrm{S}_{\mathrm{M,n,\ for\ n:1\to N}}$				
			$\mathrm{S}_{1,1}$	$\mathrm{S}_{1,2}$	...	$\mathrm{S}_{1,\mathrm{N}}$	$\mathrm{S}_{2,1}$	$\mathrm{S}_{2,2}$	...	$\mathrm{S}_{2,\mathrm{N}}$	...	$\mathrm{S}_{\mathrm{K},1}$	$\mathrm{S}_{\mathrm{K},2}$	...	$\mathrm{S}_{\mathrm{K,N}}$	
D_1	DS_1	1	$a_{1,1,1,1}$	$a_{1,1,1,2}$	...	$a_{1,1,1,N}$	$a_{1,1,2,1}$	$a_{1,1,2,2}$	...	$a_{1,1,2,N}$	...	$a_{1,1,M,1}$	$a_{1,1,M,2}$	...	$a_{1,1,M,N}$	
	DS_2	10	$a_{1,2,1,1}$	$a_{1,2,1,2}$	...	$a_{1,2,1,N}$	$a_{1,2,2,1}$	$a_{1,2,2,2}$	...	$a_{1,2,2,N}$	...	$a_{1,2,M,1}$	$a_{1,2,M,2}$	...	$a_{1,2,M,N}$	
	...															
	DS_L	100M	$a_{1,L,1,1}$	$a_{1,L,1,2}$	...	$a_{1,L,1,N}$	$a_{1,L,2,1}$	$a_{1,L,2,2}$	...	$a_{1,L,2,N}$	...	$a_{1,L,M,1}$	$a_{1,L,M,2}$	...	$a_{1,L,M,N}$	
...																
D_K	DS_1	1	$a_{K,1,1,1}$	$a_{K,1,1,2}$	...	$a_{K,1,1,N}$	$a_{K,1,2,1}$	$a_{K,1,2,2}$	...	$a_{K,1,2,N}$	...	$a_{K,1,M,1}$	$a_{K,1,M,2}$	...	$a_{K,1,M,N}$	
	DS_2	10	$a_{K,2,1,1}$	$a_{K,2,1,2}$	...	$a_{K,2,1,N}$	$a_{K,2,2,1}$	$a_{K,2,2,2}$	...	$a_{K,2,2,N}$	...	$a_{K,2,M,1}$	$a_{K,2,M,2}$	...	$a_{K,2,M,N}$	
	...															
	DS_L	100M	$a_{K,L,1,1}$	$a_{K,L,1,2}$	...	$a_{K,L,1,N}$	$a_{K,L,2,1}$	$a_{K,L,2,2}$	...	$a_{K,L,2,N}$	...	$a_{K,L,M,1}$	$a_{K,L,M,2}$	...	$a_{K,L,M,N}$	

A. *DB-ILP method*

To obtain the optimal test solution, the DB-ILP is applied. The target of the DB-ILP method is to generate a march test algorithm that can detect all validated faults while minimizing the march test length, by selecting the appropriate DB patterns and sequences. This is achieved through mathematical optimization with two steps: 1) Establish the DB-ILP table with the data of the fault modeling; 2) Formulate and solve the DB-ILP equation.

The example of the DB-ILP table is presented in TABLE I. On the top of the table, it presents all the possible DB patterns (DB_m for $m \in [1, M]$), and the sequence ($S_{m,n}$ for $m \in [1, M]$ and $n \in [1, N]$). At the left of the table, it presents the defect strength (D_k for $k \in [1, K]$) in each defect (DS_l for $l \in [1, L]$). In the center of the table, a four-dimensional binary matrix $a_{k,l,m,n} \in A$ is defined, where 'k' labels the defect name, 'l' labels the defect strength, 'm' labels the DB pattern, and 'n' labels the sequence. The total number of $a_{k,l,m,n}$ is K×L×M×N. When the defect 'k' with strength 'l' can be sensitized by sequence 'n' under DB pattern 'm', $a_{k,l,m,n} = 1$, otherwise $a_{k,l,m,n} = 0$. At the right of the table, it presents the sum of $a_{k,l,m,n}$ in this row ($\sum_{m=1}^{M}\sum_{n=1}^{N} a_{k,l,m,n}$). When this sum value is not 0, it suggests the D_k with DS_l can validate at least one fault, hence it can be sensitized in this work, otherwise, it is undetected by regular march test methods [24]. To detect them, we may need the Design for Test (DFT) [25], which is beyond the scope of this discussion. We populate this DB-ILP table with the fault modeling information.

The optimization process of selecting proper DB patterns and sequences while minimizing the march can be mathematically denoted as the DB-ILP equation:

$$\min \sum_{m=1}^{M}\left(\beta \cdot \mathrm{DB(sel)}_m \cdot \sum_{n=1}^{N} \cdot \mathrm{S(sel)}_{m,n}\right)$$

$$\text{s.t.} \begin{cases} \text{For}\,(k:1\,to\,K, l:1\,to\,L): \\ \quad \text{if } \sum_{m=1}^{M}\sum_{n=1}^{N} a_{k,l,m,n} \geq 1: \\ \qquad \sum_{n=1}^{M}\sum_{n=1}^{N} a_{k,l,m,n} \cdot \mathrm{DB(sel)}_m \cdot \mathrm{S(sel)}_{m,n} \geq 1. \end{cases}$$

The DB-ILP equation consists of two elements: the minimization statement, and the constraint. The minimization statement (first line of the equation) guarantees that appropriate DB patterns and their corresponding sequences are selected to achieve the minimal cost. Here, $DB(sel)_\mathrm{m}$ and $S(sel)_\mathrm{m,n}$ are binary values (be either '0' or '1'), indicating whether DB_m and $S_\mathrm{m,n}$ is selected in the test (i.e., '1' is selected. The β represents the cost ratio between changing the DB pattern and adding one more sequence, which is mainly determined by the circuit design and the size of the array. Here we simply assume $\beta = 100$, to make reducing the number of the DB patterns a priority. The second statement (the constraint) guarantees that all validated faults are sensitized. The 'For' loop checks every D_k with DS_l, if it is detectable by regular march test methods (i.e., $\sum_{m=1}^{M}\sum_{n=1}^{N} a_{k,l,m,n} > 0$), it must be detected by the $DB(sel)_\mathrm{m}$ and $S(sel)_\mathrm{m,n}$. Python3's PuLP optimization package is applied to solve the DB-ILP equation [26]. Notice that there may exist DB-ILP equations with multiple solutions that have the same cost. Choosing which solution depends on the actual situation.

B. *Application of DB-ILP method*

The DB-ILP method is carried out separately for two cases in Fig. 10: defects within one cell and defects between cells.

Firstly, we apply the DB-ILP for defects within one cell. Here, the DB_m refers to the two cases of NC_v (as examples in Fig. 11, MC:0 and MC:1). The output of the DB-ILP is presented as follows:

DB(sel)	S(sel)
MC:0	$1w0$, $0r0$, $1r1$

Secondly, we apply DB-ILP three times for each case when defects are between adjacent cells, as presented in Fig. 10. Here, the DB_m needs to be flexibly adjusted to (Ca, NC_v, NC_a); hence there are 8 DB situations. The output of the DB-ILP is as follows, where '-' implies DB-independent:

C_a	DB(sel)	S(sel)
C_{ac}	(1, -, -)	$0r0$, $1r1$
C_{ar}	(1, -, -)	$0r0$, $1r1$
C_{ad}	(-, -, -)	$0r0$

C. *March test algorithm generation*

To obtain the optimal march test algorithm, we need to analyze the outputs of the DB-ILP first. Sensitizing all faults when defects within one cell requires the DB pattern to be NC_v = 0, due to the magnetic coupling effect. On the other hand, sensitizing all faults when defects are between cells requires setting the C_{ac} and C_{ar} to be '1', regardless of the

Authorized licensed use limited to: TU Delft Library. Downloaded on January 30,2024 at 07:06:06 UTC from IEEE Xplore. Restrictions apply.

DB pattern (NC_v, NC_a); this implies that the read operation always sensitizes the longest defect strength range and we can ignore the magnetic coupling impact, like what has been shown in Fig. 14. Considering all the DB-ILP method outputs, we can simply apply two solid DB patterns: all cell states in '0' o include the magnetic coupling, and all cell states in '1' to include the electrical effect. Notice that this is just for our case, the STT-MRAM test design depends on the actual circuit design, the device performance, the stray field intensity, and so on. Once the write operation sensitizes the longest defect strength region when defects are between cells, we need more complex DB patterns. The march test algorithm is as follows:

$$\text{March-MRAM} = \{\Updownarrow(\text{w0})\,;\Updownarrow(\text{r0},\text{w1},\text{r1},\text{w0},\text{r0})\,; \Updownarrow(\text{w1})\,;\Updownarrow(\text{w0},\text{r0},\text{w1})\,;\Updownarrow(\text{r1})\ \}\ .$$

Here, the '⇕' indicates that addressing direction is irrelevant. The first march element initializes the STT-MRAM array to be the first solid DB pattern with all cells in '0'. The second march element firstly checks whether the initialization is succeeded, to avoid the previously operated cell state disturbing the operations on the later cell and leading to the escapes. Then, operations are applied to sensitize all validated faults when defects are within one cell. The third march element initializes the STT-MRAM array to be the second solid DB pattern with all cells in '1'. The fourth march element firstly checks the second initialization, then applies operations to sensitize all validated faults when defects are between cells. The final march element checks the final state of the device. The algorithm length is 11N. It is verified that this march test algorithm can detect all validated faults by Spice simulation.

IX. Discussion and conclusion

In this work, we put forward a systematic approach to include the *impact of magnetic coupling* into the STT-MRAM test design for contact and interconnect defects. Firstly, we offer the method to incorporate the magnetic coupling effect into the defect-free STT-MRAM array circuit. Then, we define the defect space and perform the fault modeling. It presents that if the STT-MRAM test ignores or does not properly include the magnetic coupling, it gets either a high escape rate or a low time efficiency. Finally, we proposed the test method and generate the optimal march test algorithm.

There are some limitations and possible extensions in this work. Firstly, we have not considered the physical layout design, which is an essential issue in the real industrial test design. Secondly, we only investigate the static faults with one operation, while ignoring the dynamic faults with multiple operations. Thirdly, although we proposed the method to generate the optimal march test solution, the march algorithm is actually a little too long; there may exist other test methods, like the DFT, that can improve the test efficiency. Fourthly, the method of transforming the magnetic field to an 'equivalent current source' can actually be applied to all types of the magnetic field, which will helpful in simulating the MTJ working under the magnetic field. Our future work will focus on addressing these limitations and investigating the possible extensions.

Acknowledgements

This work is supported by IMEC's Industrial Affiliation Program on STT-MRAM devices.

References

[1] L. Wei *et al.*, "13.3 A 7Mb STT-MRAM in 22FFL FinFET Technology with 4ns Read Sensing Time at 0.9V Using Write-Verify-Write Scheme and Offset-Cancellation Sensing Technique," in *ISSCC*, 2019, pp. 214–216.
[2] S. Tehrani, "Status and Outlook of MRAM Memory Technology (Invited)," in *IEDM*, 2006, pp. 1–4.
[3] K. Lee *et al.*, "1Gbit High Density Embedded STT-MRAM in 28nm FDSOI Technology," in *IEDM*, 2019, pp. 2.2.1–2.2.4.
[4] W.J. Gallagher *et al.*, "22nm STT-MRAM for Reflow and Automotive Uses with High Yield, Reliability, and Magnetic Immunity and with Performance and Shielding Options," in *IEDM*, 2019, pp. 2.7.1–2.7.4.
[5] S. Aggarwal *et al.*, "Demonstration of a Reliable 1 Gb Standalone Spin-Transfer Torque MRAM For Industrial Applications," in *IEDM*, 2019, pp. 2.1.1–2.1.4.
[6] J. Azevedo *et al.*, "A complete resistive-open defect analysis for thermally assisted switching MRAMs," in *VLSI*, vol. 22, no. 11. IEEE, 2014, pp. 2326–2335.
[7] S.M. Nair *et al.*, "Defect injection, fault modeling and test algorithm generation methodology for STT-MRAM," in *ITC*, 2018, pp. 1–10.
[8] A. Chintaluri *et al.*, "A model study of defects and faults in embedded spin transfer torque (STT) MRAM arrays," in *ATS*, 2015, pp. 187–192.
[9] I. Yoon *et al.*, "EMACS: Efficient MBIST architecture for test and characterization of STT-MRAM arrays," in *ITC*, 2016, pp. 1–10.
[10] I. Yoon *et al.*, "Modeling and analysis of magnetic field induced coupling on embedded STT-MRAM arrays," *IEEE T. COMPUT. AID. D.*, vol. 37, pp. 337–349, 2017.
[11] S.M. Nair *et al.*, "VAET-STT: Variation aware STT-MRAM analysis and design space exploration tool," *IEEE T. COMPUT. AID. D.*, vol. 37, pp. 1396–1407, 2017.
[12] S. Hamdioui *et al.*, "An experimental analysis of spot defects in SRAMs: realistic fault models and tests," in *ATS*, 2000.
[13] A.J. van de Goor *et al.*, "Disturb neighborhood pattern sensitive fault," in *VTS*, 1997, pp. 37–45.
[14] G. Radhakrishnan *et al.*, "Monitoring aging defects in STT-MRAMs," *IEEE T. COMPUT. AID. D.*, vol. 39, pp. 4645–4656, 2020.
[15] L. Wu *et al.*, "Impact of magnetic coupling and density on stt-mram performance," in *DATE*, 2020, pp. 1211–1216.
[16] M. Taouil *et al.*, "Device Aware Test for Memory Units," 2021, in European patent EP4026128A1.
[17] Y.H. Wang *et al.*, "Impact of stray field on the switching properties of perpendicular MTJ for scaled MRAM," in *IEDM*, 2012, pp. 29.2.1–29.2.4.
[18] A.V. Khvalkovskiy *et al.*, "Basic principles of STT-MRAM cell operation in memory arrays," *J. Phys. D: Appl. Phys*, vol. 46, p. 139601, 2013.
[19] S. Salehi *et al.*, "Survey of STT-MRAM cell design strategies: Taxonomy and sense amplifier tradeoffs for resiliency," *ACM J. EMERG. TECH. COM.*, vol. 13, pp. 1–16, 2017.
[20] S. Hamdioui *et al.*, "Memory fault modeling trends: A case study," *J. Electron. Testing*, vol. 20, pp. 245–255, 2004.
[21] R. Koch *et al.*, "Time-resolved reversal of spin-transfer switching in a nanomagnet," *Phys. Rev. Lett.*, vol. 92, p. 088302, 2004.
[22] W. Skowroński *et al.*, "Backhopping effect in magnetic tunnel junctions: Comparison between theory and experiment," *JAP*, vol. 114, p. 233905, 2013.
[23] ASU, "Predictive Technology Model (PTM)," 2012.
[24] M. Fieback *et al.*, "Defects, fault modeling, and test development framework for rrams," *ACM J. Emerg. Technol. Comput. Syst.*, vol. 18, pp. 1–26, 2022.
[25] S. Taghipour *et al.*, "CD-DFT: A current-difference design-for-testability to detect short defects of STT-MRAM under process variations," *IEEE Trans. Device Mat. Rel.*, vol. 21, pp. 436–443, 2021.
[26] S. Mitchell *et al.*, "Pulp: a linear programming toolkit for python. 2011," *URL https://code. google. com/p/pulp-or*, 2011.

Authorized licensed use limited to: TU Delft Library. Downloaded on January 30,2024 at 07:06:06 UTC from IEEE Xplore. Restrictions apply.